Supplement of

How does a warm and low-snow winter impact the snow cover dynamics in a humid and discontinuous boreal forest? An observational study in eastern Canada.

Benjamin Bouchard et al.,

Correspondence to: Benjamin Bouchard (benjamin.bouchard.1@ulaval.ca)

S1: Heating curve analysis

The heating curve analysis is derived from Domine et al. (2015). Following their method, we evaluated the temperature change on a logarithmic time scale for heating periods between 40 and 100 seconds and selected the steepest slope. The inverse of the slope yields the value of k_s. The R^2 of the slope must be higher than 0.98 and we kept the value of k_s if there was no sign of convection on the heating curve, as described by Domine et al. (2015). Figure S1 shows an example of heating curve analysis.

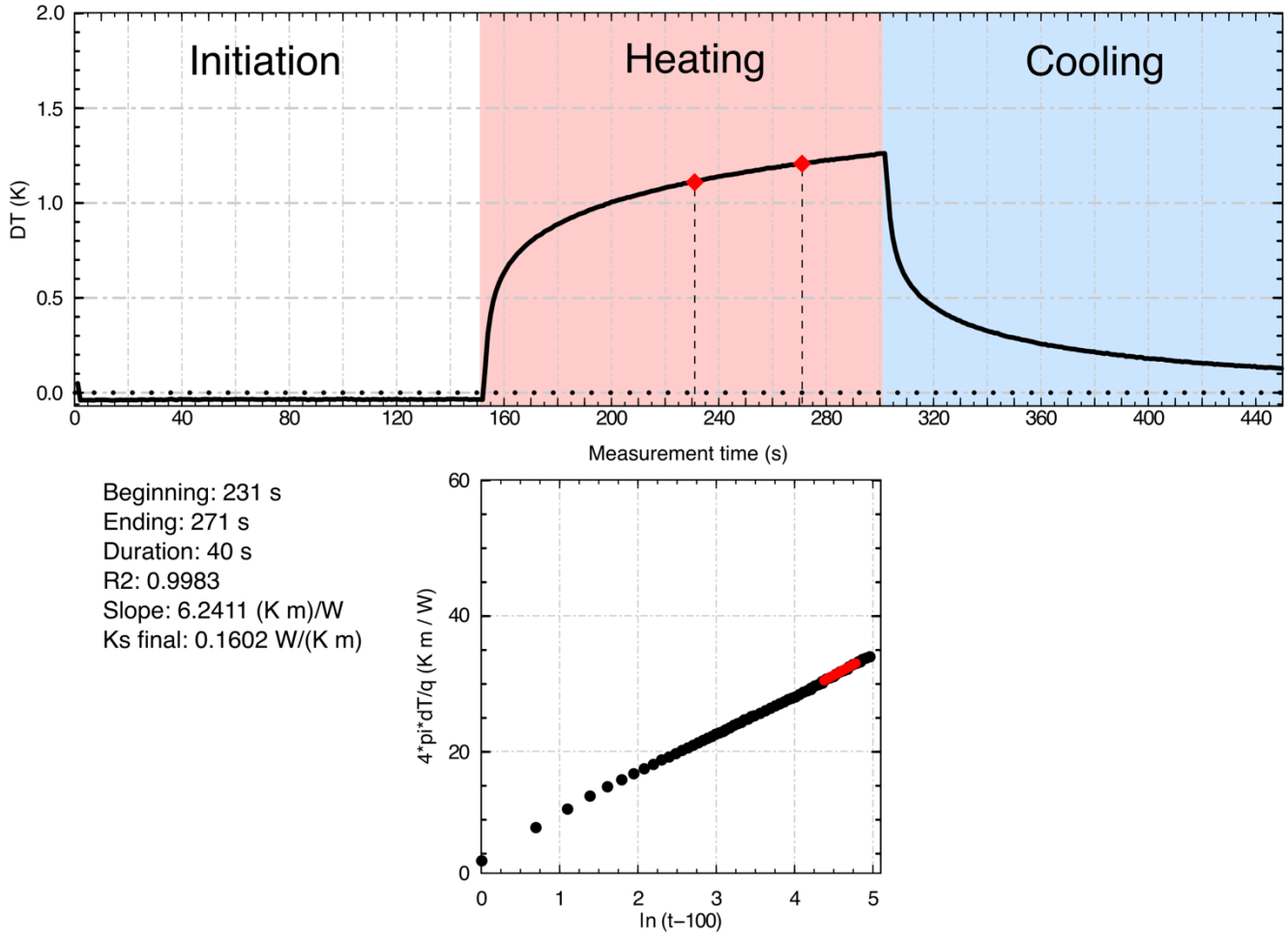

Figure S1: Heating curve analysis for the 80-cm needle from the monitoring station in the medium gap on 2 February 2022. In this example, we selected a period of 40 seconds that started at 231 seconds. The slope is 6.24 K m W^{-1} which gives a k_s of 0.16 W m^{-1} K^{-1}. Since R^2 is greater than 0.98 and no convection was detected, the measurement is considered valid.

S2: Data gap filling

S2.1 Snow height in medium gap (15 November 2020 to 22 December 2020)

Since snow heights in medium and small gaps are similar, we filled this gap using snow height measurement in the small gap. We adjusted gap-filled snow height proportionally to the height difference between both stations at the end of the gap.

S2.2 Snow height under the canopy (26 February 2022 to 14 May 2022)

Step 1: we computed the ratio between the snow heights measured under the canopy and inside small gap. We applied this ratio to the snow height in the small gap for the period of 26 February to 14 May 2022. Step 2: we shifted up the resulting snow height so it equals the canopy snow height at the beginning of the gap. On 24 April 2022, snow height started declining consistently. Step 3: we corrected the replacement snow height from that date onward proportionally to the height difference at the end of the gap. Figure S2 shows the steps of this gap-filling.

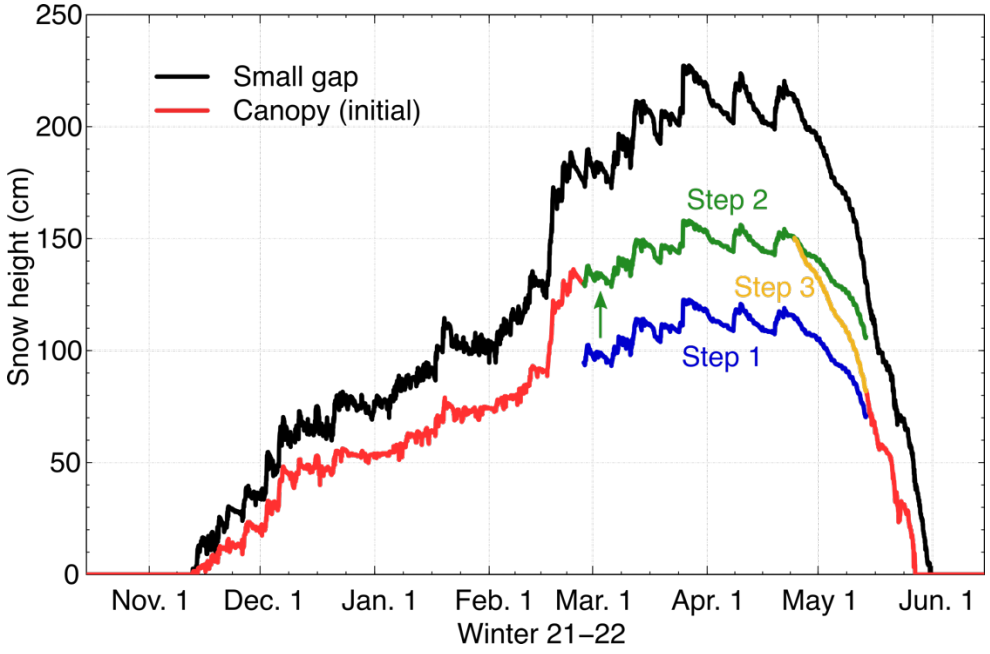

Figure S2: Step-by-step method to replace the gap in the winter 2021–22 canopy snow height time series.

S2.3 Snow surface temperature in the small gap (Winter 21-22)

We did a linear regression of snow surface temperature (T_{surf}) between the medium and small gaps and between the canopy and the small gap for the snow cover period of winter 2020–21. We applied this regression to T_{surf} in large gap and under the canopy for winter 2021–22 and computed the average between both to estimate the T_{surf} in the small gap. Figure S3 shows the linear models.

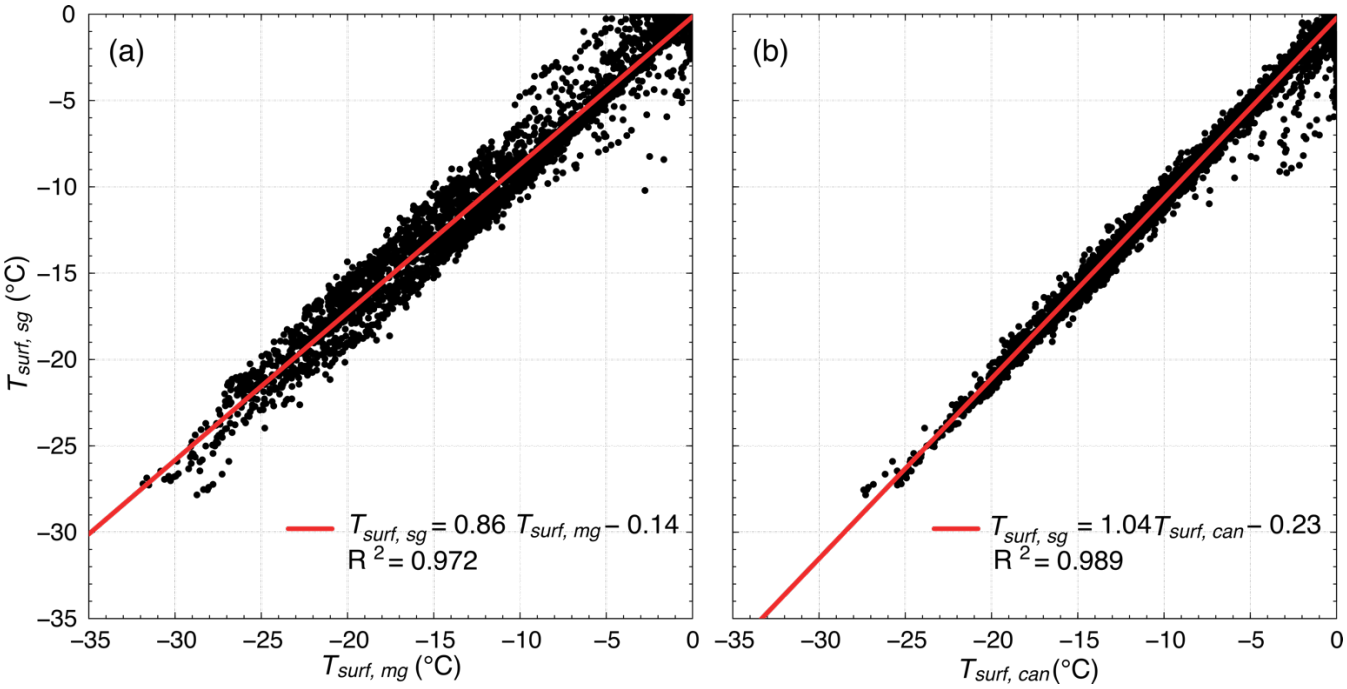

Figure S3: Linear regression of snow surface temperature between medium and small gaps (a) and between canopy and small gap (b) for snow cover period of winter 2020–21.

S2.4 Snow surface temperature and air temperature under the canopy (28 April 2022 to 14 May 2022)

To fill the gap of T_{surf} under the canopy, we did a linear regression with T_{surf} in the medium gap for winter 20-21. We applied the linear regression to SST in medium gap to estimate the T_{surf} under the canopy for the missing period of winter 2021–22. We used the same method to replace missing air temperature (T_a) under the canopy in winter 2021–22 but using T_a in small gap instead of medium gap. We used the T_{surf} of the medium gap instead of small gap to avoid using gap-filled data to replace missing T_{surf} under the canopy. Figure S4 shows the linear models.

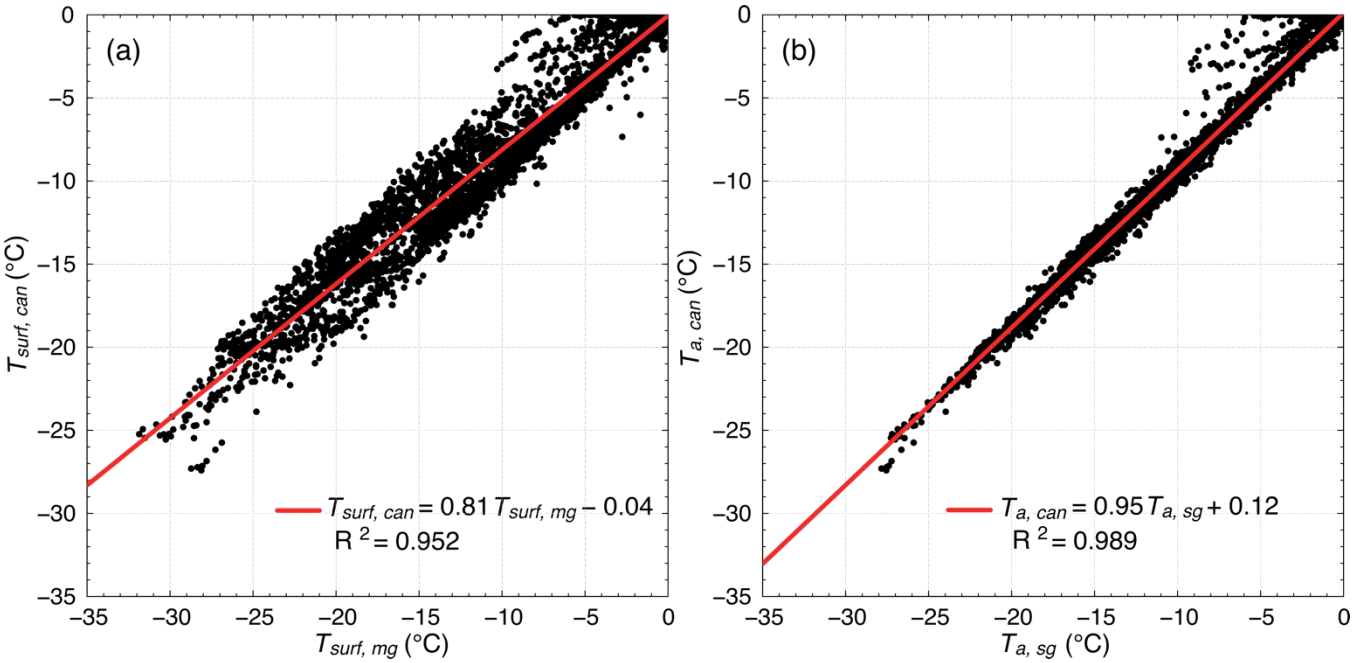

Figure S4: Linear regressions of snow surface temperature between medium gap and canopy (a) and of air temperature between canopy and small gap (b) for snow cover period of winter 2020–21.

S3: Observed and estimated snow water equivalent

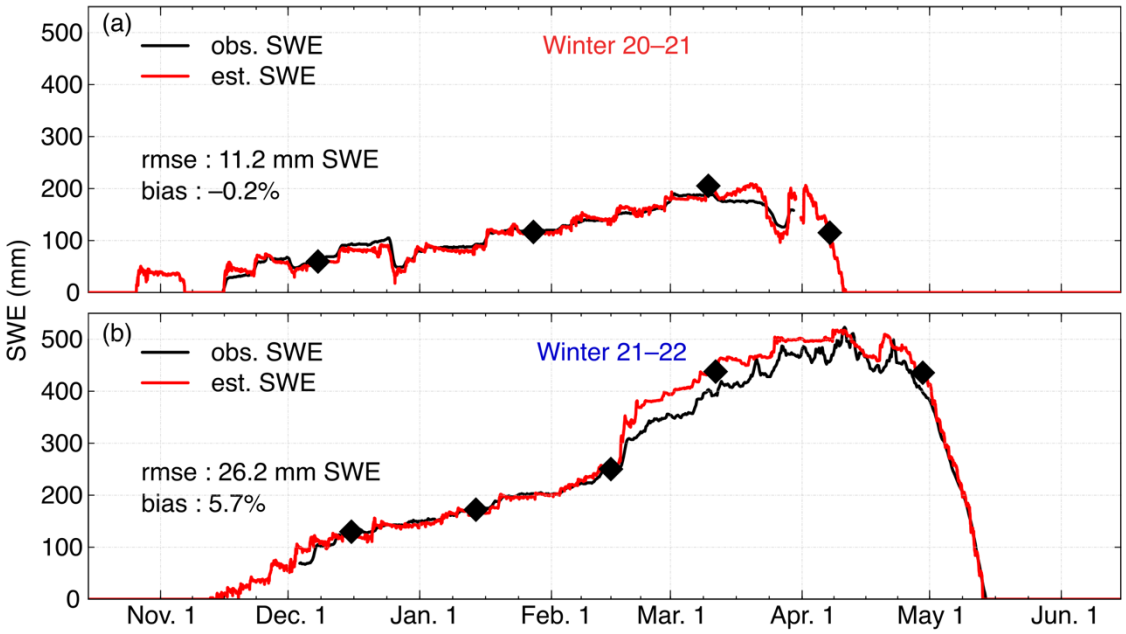

Figure S5: Comparison between the SWE monitored by the CS725 and the SWE derived from density profiles interpolation and snow height measurement in NEIGE site. The RMSE corresponds to 5.9% of the maximum SWE in winter 2020–21 and to 5.0% of the max SWE in winter 2021–22. Black diamonds show the corresponding date of the density profile measurements.

S4: Albedo classes

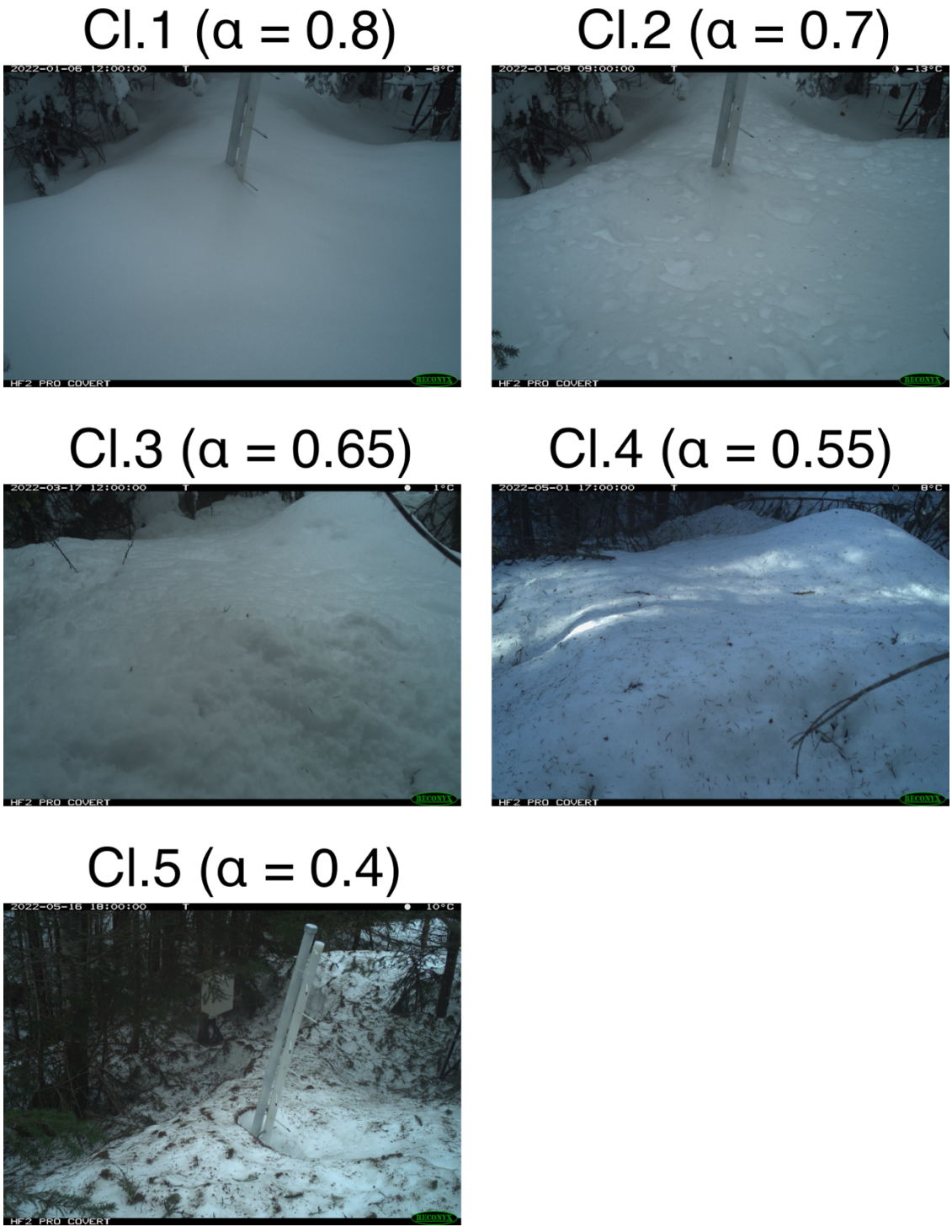

Figure S6: Photo of each albedo (α) classes as taken by the timelapse camera installed at the small gap station

S5: Estimation of k_s

We obtained 15 observations of snow density and grain shape that we linked to a k_s measured using fixed needle probes and corrected based on Fourteau et al. (2022). Observations were compared to Eq. 18 from Fourteau et al. (2021) as shown on Figure S7.

$$k_s = \begin{cases} 2.564\left(\frac{\rho_s}{\rho_i}\right)^2 - 0.059\left(\frac{\rho_s}{\rho_i}\right) + 0.0205 & \overline{T_s} = 223\ K \\ 2.172\left(\frac{\rho_s}{\rho_i}\right)^2 + 0.015\left(\frac{\rho_s}{\rho_i}\right) + 0.0252 & \overline{T_s} = 248\ K \\ 1.985\left(\frac{\rho_s}{\rho_i}\right)^2 + 0.073\left(\frac{\rho_s}{\rho_i}\right) + 0.0336 & \overline{T_s} = 263\ K, \\ 1.883\left(\frac{\rho_s}{\rho_i}\right)^2 + 0.107\left(\frac{\rho_s}{\rho_i}\right) + 0.0386 & \overline{T_s} = 268\ K \\ 1.776\left(\frac{\rho_s}{\rho_i}\right)^2 + 0.147\left(\frac{\rho_s}{\rho_i}\right) + 0.0455 & \overline{T_s} = 273\ K \end{cases} \quad (1)$$

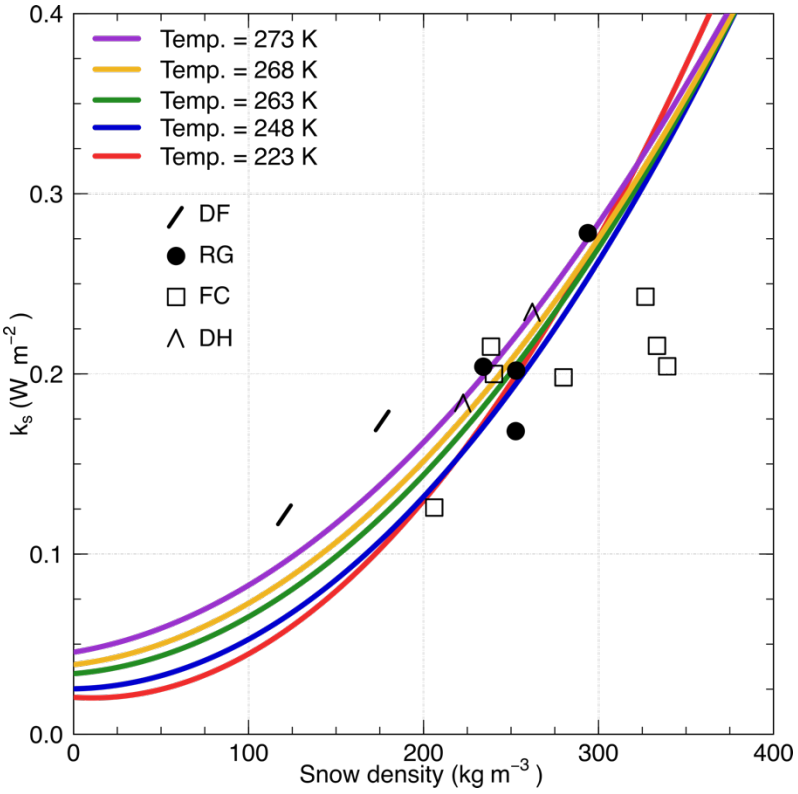

Figure S7: Observations of k_s and snow density compared with temperature-dependant equations from Fourteau et al. (2021). The correlation coefficient between the observations and equation 1 is 0.70. The observed grain shape is also shown (DF – Decomposed and Fragmented precipitation particles; RG – Rounded Grains; FC – Facetted Crystals; DH – Depth Hoar).

65 **S6: Snow pit observations**

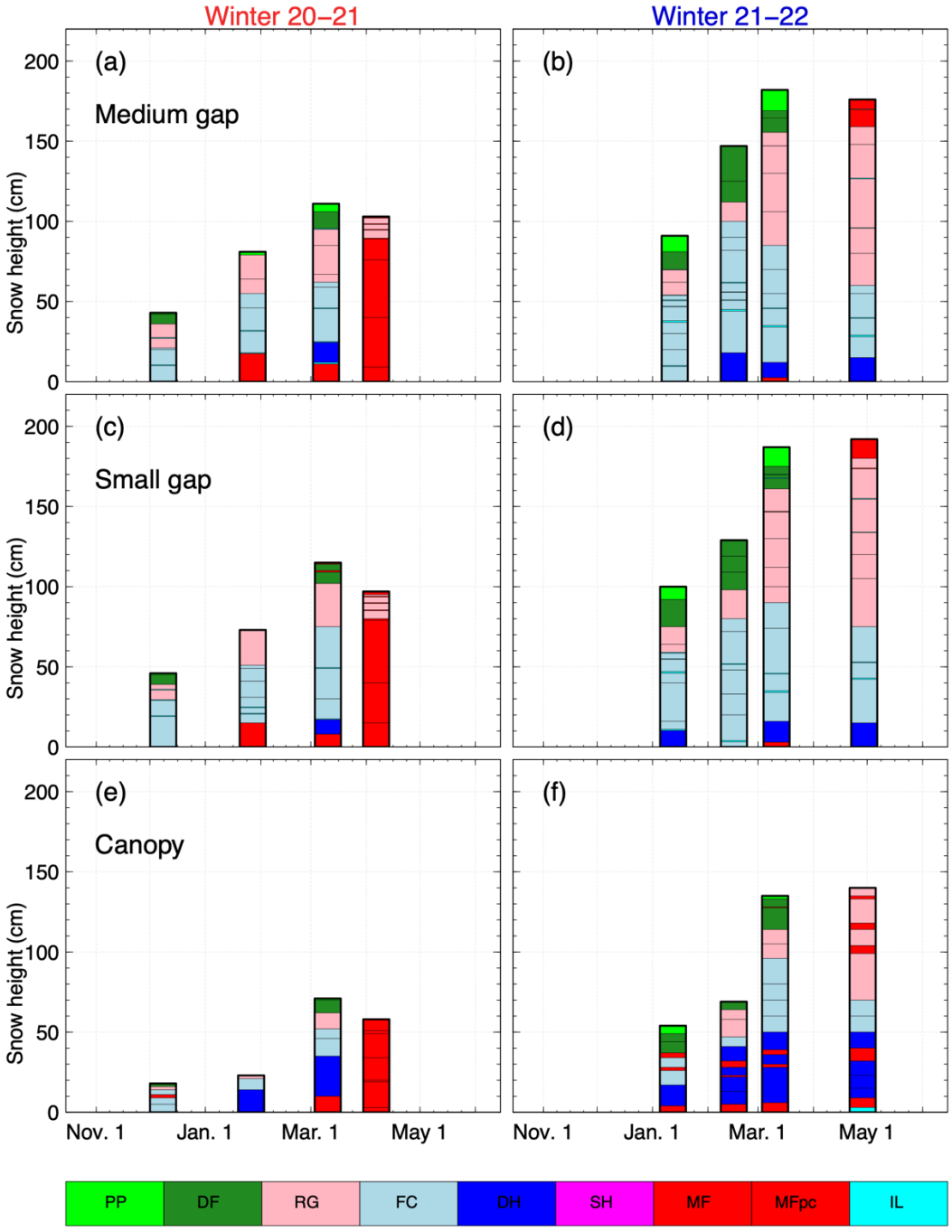

Figure S8: Snowpack stratigraphy from snow pit measurements in the medium and small gaps, and under the canopy during winters 2020–21 and 2021–22. The colour coding follows that of the International Classification for Seasonal Snow on the Ground (Fierz et al., 2009).

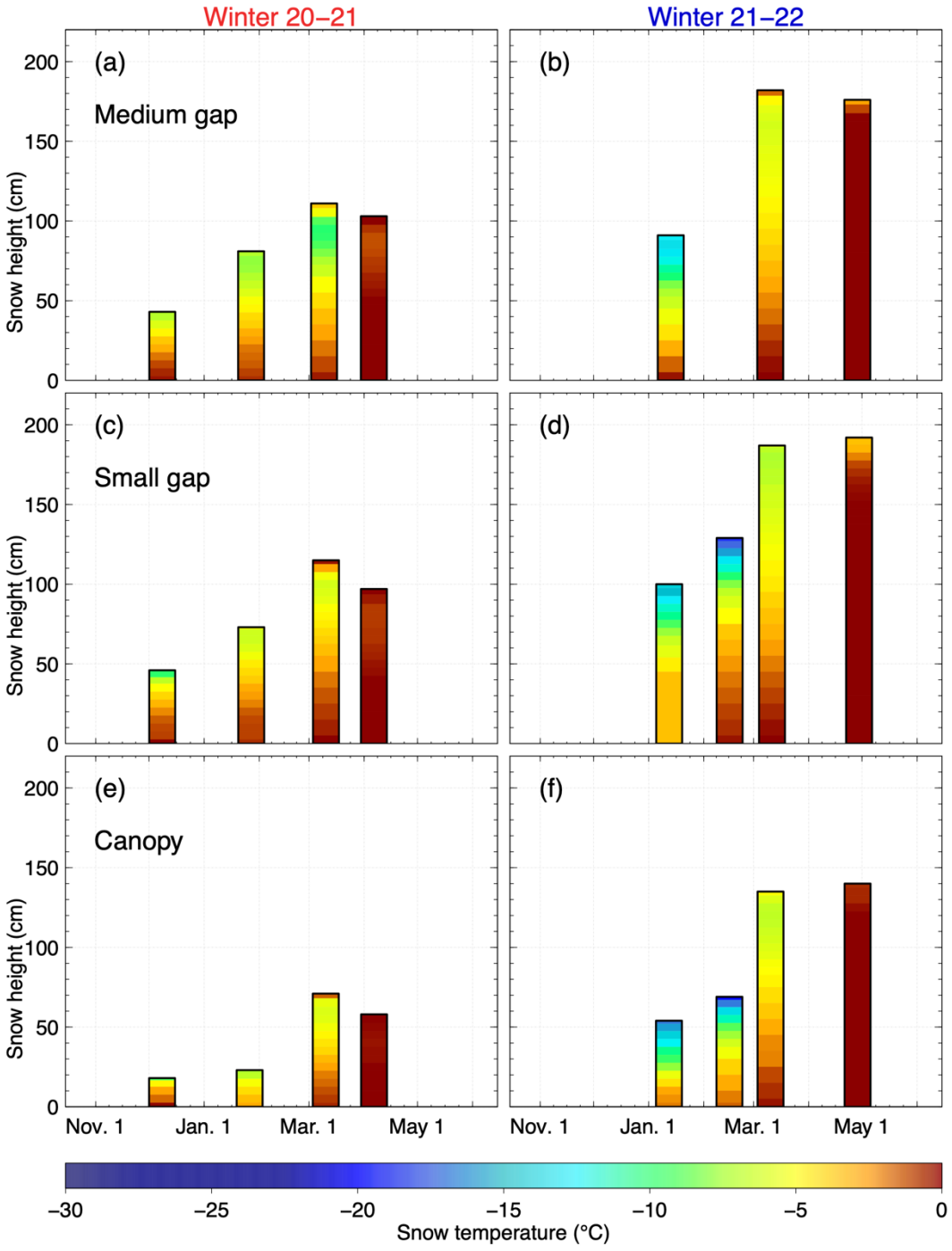

Figure S9: Temperature profiles from snow pit measurements in the medium and small gaps, and under the canopy during winters 2020–21 and 2021–22.

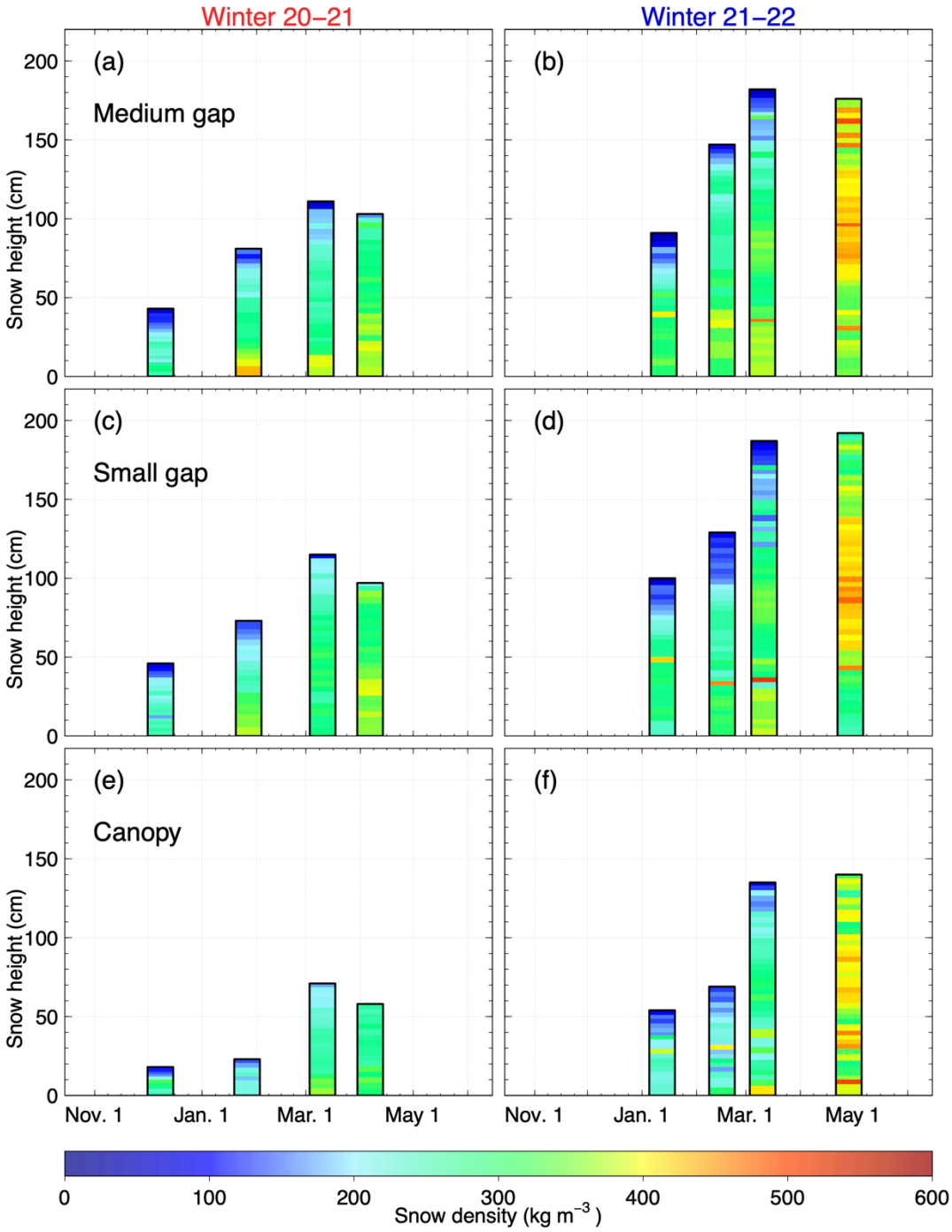

Figure S10: Snow density profiles from snow pit measurements in the medium and small gaps, and under the canopy during winters 2020–21 and 2021–22.

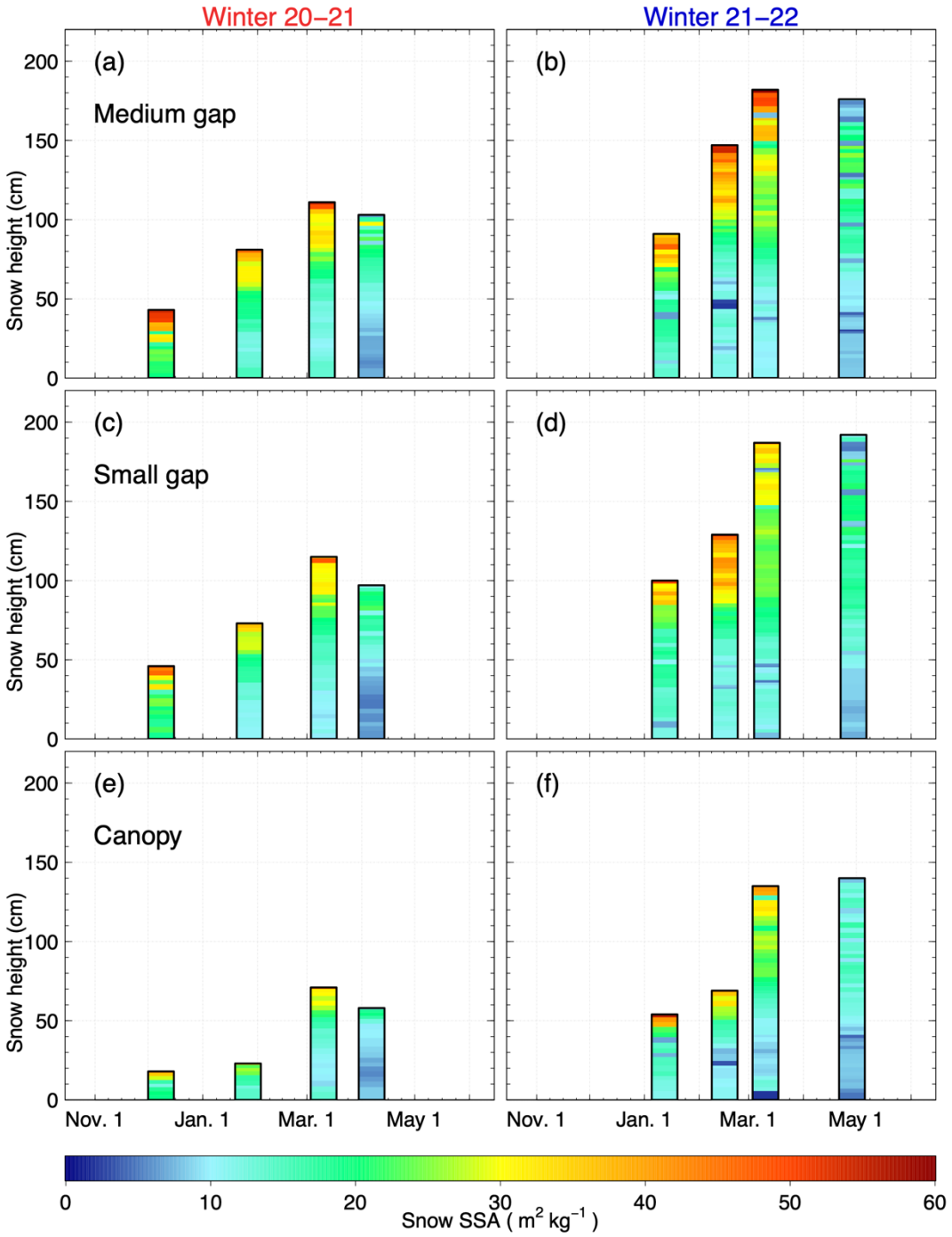

Figure S11: Snow SSA profiles from snow pit measurements in the medium and small gaps, and under the canopy during winters 2020–21 and 2021–22.

References

Domine, F., Barrere, M., Sarrazin, D., Morin, S., and Arnaud, L.: Automatic monitoring of the effective thermal conductivity of snow in a low-Arctic shrub tundra, Cryosphere, 3, 1265-1276, http://dx.doi.org/10.5194/tc-9-1265-2015, 2015.

Fierz, C., Armstrong, R. L., Durand, Y., Etchevers, P., Greene, E., McClung, D. M., Nishimura, K., Satyawali, P. K., and Sokratov, S. A.: The International Classification for Seasonal Snow on the Ground (IC-SSG), IHP-VII Technical Documents in Hydrology, UNESCO-IHP, Paris, France, 2009.

Fourteau, K., Domine, F., and Hagenmuller, P.: Impact of water vapor diffusion and latent heat on the effective thermal conductivity of snow, Cryosphere, 15, 2739-2755, https://doi.org/10.5194/tc-15-2739-2021, 2021.

Fourteau, K., Hagenmuller, P., Roulle, J., and Domine, F.: On the use of heated needle probes for measuring snow thermal conductivity, J. Glaciol., 68, 705-719, http://dx.doi.org/10.1017/jog.2021.127, 2022.